

# Enhancing Object Discovery for Unsupervised Instance Segmentation and Object Detection

Xingyu Feng<sup>1\*</sup>, Hebei Gao<sup>2\*</sup>, Hong Li<sup>1†</sup>

<sup>1</sup>College of Computer Science and Artificial Intelligence, Wenzhou University

<sup>2</sup>Oujiang Laboratory (Zhejiang Lab for Regenerative Medicine, Vision and Brain Health), Eye Hospital, Wenzhou Medical University  
24451352011@stu.wzu.edu.cn, gaohebei@ojlab.ac.cn, lihong@wzu.edu.cn

## Abstract

We propose **Cut-Once-and-LEaRn** (COLER), a simple approach for unsupervised instance segmentation and object detection. COLER first uses our developed CutOnce to generate coarse pseudo labels, then enables the detector to learn from these masks. CutOnce applies Normalized Cut only once and does not rely on any clustering methods, but it can generate multiple object masks in an image. We have designed several novel yet simple modules that not only allow CutOnce to fully leverage the object discovery capabilities of self-supervised models, but also free it from reliance on mask post-processing. During training, COLER achieves strong performance without requiring specially designed loss functions for pseudo labels, and its performance is further improved through self-training. COLER is a zero-shot unsupervised model that outperforms previous state-of-the-art methods on multiple benchmarks. We believe our method can help advance the field of unsupervised object localization.

## Introduction

In computer vision, segmentation tasks heavily rely on large-scale manual annotations, which significantly limits the development speed of the field. To reduce dependence on labeled data, researchers have begun exploring weakly-supervised or unsupervised approaches (Simeoni et al. 2025). This work focuses on exploring how to perform unsupervised instance segmentation and object detection efficiently. Found (Siméoni et al. 2022) and FreeSolo (Wang et al. 2022a) established the two-stage framework for unsupervised segmentation: generating pseudo labels followed by training a detector using them.

In recent years, methods that use self-supervised models (SSM) to extract image features and then apply Normalized Cut (NCut) (Shi and Malik 2000) to generate pseudo labels have made impressive progress, outperforming many other approaches. TokenCut (Wang et al. 2022b), MaskCut (Wang et al. 2023), and VoteCut (Arica et al. 2024) all use the DINO (Caron et al. 2021) model to extract features and produce reliable pseudo labels, achieving significant advances in unsupervised object localization field. DiffCut (Couairon

Train-Free Mask Generators	MaskCut	VoteCut	Ours
Normalized Cut #nums	3	1	1
clustering method	×	✓	×
post-process mask	✓	✓	×
self-supervised #models	1	6	1
max #objects detected	3	10	>10
mask generation time (s/img)	5.6	2.4	<b>0.24</b>
Pseudo Mask Learners	CutLER	CuVLER	Ours
pseudo mask loss function	✓	✓	×
AP <sub>50</sub> <sup>mask</sup> on COCO val2017	18.9	19.3	<b>20.1</b>

Table 1: **Comparison of COLER (row 8) with previous popular methods.** The table includes CutLER, CuVLER, and their corresponding pseudo mask generators. The last row reports zero-shot evaluation results on COCO val2017, and our method achieves higher accuracy and faster speed.

et al. 2024) employs a diffusion UNet (Ronneberger, Fischer, and Brox 2015) encoder for feature extraction, targeting unsupervised semantic segmentation.

The NCut paper (Shi and Malik 2000) recommends two approaches for extending from single-object to multi-object segmentation. One approach is to perform NCut once, using the top- $n$  eigenvectors as an  $n$ -dimensional indicator vector, followed by clustering (e.g., K-Means) to segment multiple objects. VoteCut (Arica et al. 2024) adopts a clustering-based approach and generates masks using only the second smallest eigenvector. However, clustering methods require specifying the number of clusters, which reduces the generality of such approaches. The other approach is to recursively partition the separated groups, that is, to further split the current foreground or background regions. MaskCut (Wang et al. 2023) adopts this strategy by recursively partitioning the background. However, this approach clearly suffers from error accumulation as the number of recursive steps increases. These two types of methods have low computational efficiency, hindering their application and further exploration in related fields.

This paper uses NCut to segment multiple objects, but differs from the two types of methods mentioned above. Our CutOnce neither relies on multiple applications of NCut nor

\*Equal contribution.

†Corresponding author.

on clustering methods when discovering multiple objects. In short, by applying NCut only once and designing two object discovery enhancement modules, CutOnce can segment multiple objects from an image, which is the origin of its name. Additionally, with a feature-ranking-based module, the method can detect over 10 object masks (examples are shown in the Appendix). CutOnce does not require computationally expensive methods such as Conditional Random Field (CRF) (Krähenbühl and Koltun 2011). By fully leveraging the feature, geometric, and localization cues learned by SSM, it achieves promising results. Table 1 summarizes the key properties of CutOnce and popular existing methods (Wang et al. 2023; Arica et al. 2024), showing that CutOnce not only detects more objects but also generates annotations up to  $10\times$  faster. COLER uses CutOnce’s annotations for training and achieves good performance through self-training alone, without the need to design specialized loss functions to handle errors in the “ground truth” provided by pseudo masks.

The contributions of this paper can be summarized as follows: 1) We develop an efficient tool, CutOnce, for generating coarse masks. 2) We train a detector, COLER, using pseudo masks generated by CutOnce. COLER is a zero-shot model that outperforms previous methods across multiple datasets.

## Related Work

**Self-Supervised Vision Transformer.** Self-supervised models are capable of learning deep features without human annotations or supervision. ViT (Dosovitskiy et al. 2020) captures long-range dependencies between different regions in images through a global self-attention mechanism, making it easier to focus on semantically consistent target regions compared to CNNs. DINO (Caron et al. 2021) combines both advantages, playing a key role in advancing unsupervised object localization. It adopts a teacher-student training framework and introduces a novel contrastive learning strategy that compares features from the original image and its random crops to learn stronger visual representations. Thanks to the built-in spatial attention mechanism of the ViT architecture, DINO’s attention maps can be directly used for localization and have shown clear advantages over previous methods. By further processing DINO’s attention maps, more precise object regions can be obtained. And many methods (Wang et al. 2022b, 2023; Arica et al. 2024; Sick et al. 2024) have been developed based on this idea, achieving significant progress in their respective fields.

**Unsupervised Instance Segmentation and Object Detection.** The following methods all utilize unsupervised object localization, which is then applied to instance segmentation and object detection tasks. Early approaches do not use NCut (Shi and Malik 2000), while later ones adopt it.

LOST (Siméoni et al. 2021) is the first to localize objects by leveraging the final layer CLS token from a pre-trained transformer DINO (Caron et al. 2021) and computing patch-wise similarity within single image, but it can only localize one object. MOST (Rambhatla et al. 2023) extends this to multiple objects through entropy-based box analy-

sis and clustering. FreeSOLO (Wang et al. 2022a) uses features from DenseCL (Wang et al. 2020) to generate a set of queries and keys which are convolved to produce segmentation masks and also supports multiple object localization. These methods do not rely on NCut and their robustness on large-scale datasets remains unconvincing.

TokenCut (Wang et al. 2022b) is the first to apply NCut to features extracted by DINO, significantly improving the quality of pseudo labels, but it can only segment single instance. CutLER (Wang et al. 2023) recursively applies NCut on one image to generate masks for multiple instances. CuVLER (Arica et al. 2024) uses multiple self-supervised models to generate diverse mask proposals and selects the best masks through clustering and pixel-wise voting. In addition, it assigns a confidence score to each pseudo mask. Table 1 presents the properties of the above methods and compares them with ours. CutS3D (Sick et al. 2024) introduces 3D information to enhance instance segmentation in 2D images, showing certain advantages in handling overlapping or connected objects and demonstrating strong potential for real-world applications. DiffNCut (Liu and Gould 2024) proposes Differentiable Normalized Cuts. In other words, it uses NCut to propagate gradients and fine-tune DINO. Since NCut enhances object discovery, methods that use it clearly outperform those that do not.

## Method

This chapter introduces a novel pipeline called Cut-Once-and-LEaRn (COLER), designed for unsupervised instance segmentation and object detection. We first propose CutOnce, a training-free method that efficiently generates masks for multiple objects. Built upon prior work, CutOnce enhances object discovery by optimizing the edge weighting scheme and introducing a boundary enhancement strategy in the NCut algorithm. In addition, it incorporates a feature-ranking-based filtering module to retain a sufficient number of valuable object masks. Finally, we train a detector using the masks generated by CutOnce and further improve its performance through a self-training strategy.

### Preliminaries

**Normalized Cut.** NCut (Shi and Malik 2000) formulates image segmentation as a graph partitioning problem. It constructs a fully connected undirected graph  $G = (V, E)$  by representing the image as a set of nodes, where each pair of nodes is connected by an edge with weight  $w_{ij}$  indicating their similarity. NCut minimizes the cost of partitioning the graph into two subgraphs by solving a generalized eigenvalue system. Solving

$$(\mathbf{D} - \mathbf{W})\mathbf{x} = \lambda\mathbf{D}\mathbf{x} \quad (1)$$

yields a set of  $N \times N$  eigenvectors  $\mathbf{x}$ , where  $N$  denotes the number of nodes. Here,  $\mathbf{D}$  is an  $N \times N$  diagonal matrix with  $d_{ii} = \sum_j w_{ij}$ , and  $\mathbf{W}$  is an  $N \times N$  symmetric matrix representing the adjacency matrix of edge weights.

**TokenCut and MaskCut.** Our CutOnce is based on the overall workflow of TokenCut (Wang et al. 2022b), with

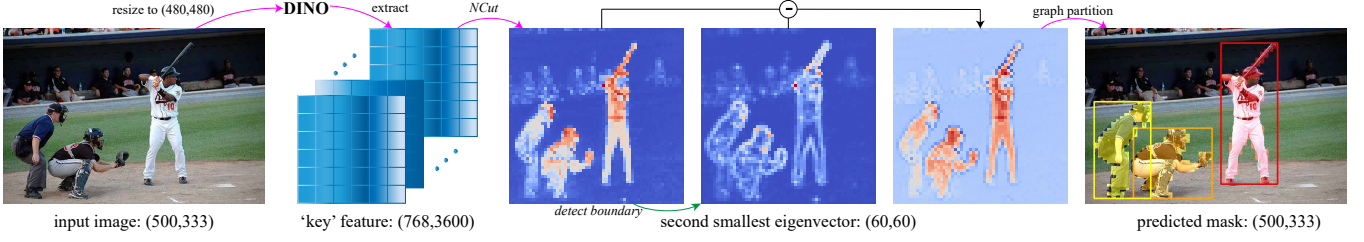


Figure 1: **Overview of CutOnce.** First, the resized image is processed by DINO to extract the “key” features. Then, the NCut algorithm is applied to obtain the second smallest eigenvector. Next, the original eigenvector is used to compute the boundary eigenvector, and the two are subtracted element-wise to produce the boundary-enhanced eigenvector. Finally, the enhanced eigenvector is partitioned to obtain the segmentation masks.

some implementation details adopting the design of Mask-Cut (Wang et al. 2023). The following describes the consistent parts of CutOnce with existing methods.

First, the input image is passed through a single self-supervised model to extract the “key” features from the last attention layer, denoted as  $\mathbf{K} \in \mathbb{R}^{D \times N}$ , where  $D$  is the feature dimension and  $N$  is the number of nodes. These features encode the spatial information captured by ViT (Dosovitskiy et al. 2020), so the cosine similarity between them can be used to calculate the elements in  $\mathbf{W}$ :

$$w_{ij} = \cos(\mathbf{k}_i, \mathbf{k}_j) = \frac{\mathbf{k}_i^T \mathbf{k}_j}{\|\mathbf{k}_i\|_2 \|\mathbf{k}_j\|_2} \quad (2)$$

where  $\mathbf{k}_i$  is the “key” feature of patch  $i$ .

Then, the second smallest eigenvector  $\mathbf{y}_1$  is obtained from the solution of Equation 1, which can be viewed as an enhanced attention map. When the splitting threshold is set to  $\bar{y}_1 = \frac{1}{N} \sum_i \mathbf{y}_1^i$ ,  $\mathbf{y}_1$  can be effectively divided into background and foreground. To determine which side corresponds to the foreground, we analyze the distribution of  $\mathbf{y}_1$  on the ImageNet (Deng et al. 2009) and COCO (Lin et al. 2014) datasets and adopt two criteria: 1) The foreground set should include fewer than three of the four corners of the image, based on the object-centric prior (Maji, Vishnoi, and Malik 2011), which is also used in MaskCut. 2) When  $|\max(\mathbf{y}_1)| < |\min(\mathbf{y}_1)|$ , this follows the same setting as TokenCut. If either of the above conditions is satisfied (with condition 1 taking priority), the eigenvector used for mask partitioning  $\mathbf{v}$  is set to  $-\mathbf{y}_1$ ; otherwise, it is set to  $\mathbf{y}_1$ . Finally, elements in  $\mathbf{v}$  greater than the split point are considered foreground, while those below are regarded as background.

Existing methods have paved the way for our research, but the following limitations remain urgent to address: 1) Instead of refining masks during the NCut stage, they rely on CRF (Krähenbühl and Koltun 2011) in the post-processing step. 2) The maximum number of detectable objects per image is often unsatisfactory. 3) They are generally time-consuming when handling multiple objects.

### CutOnce: Efficient Mask Generator

Given the limitations of prior works, we aim to address the following challenges: 1) How to produce more accurate foreground boundaries. 2) How to enable the NCut algorithm to discover multiple objects rather than focusing on

a single one. 3) How to segment more objects without introducing too many incorrect masks. To this end, we introduce three simple yet effective modules to tackle these issues.

**Density-Tune Cosine Similarity.** Previous methods (Wang et al. 2022b, 2023; Arica et al. 2024) compute the edge weight matrix  $\mathbf{W}$  solely based on the cosine similarity between nodes, ignoring the variations in feature density across different image regions. This often leads to over-activation in certain areas, which negatively affects boundary localization. To address this issue, we propose a local-density-aware temperature modulation for cosine similarity. The core idea is to adaptively adjust the temperature parameter in similarity computation based on the local density of feature points.

For the convenience of subsequent calculations, the deep learning features  $\mathbf{K}$  are first normalized. The elements of the adaptive edge weight matrix are defined as:

$$w_{ij} = \frac{\cos(\mathbf{k}_i, \mathbf{k}_j)}{T_{ij}} = \frac{\mathbf{k}_i^T \mathbf{k}_j}{T_0 + \alpha \cdot \frac{\rho_i + \rho_j}{2}} \quad (3)$$

where  $T_{ij}$  denotes the adaptive temperature parameter,  $T_0$  is the base temperature,  $\alpha$  is the modulation parameter, and  $\rho_i$  and  $\rho_j$  represent the local densities of feature points  $i$  and  $j$ , respectively.

The local density is computed by first calculating the pairwise cosine similarity matrix  $\mathbf{S} = \mathbf{K}\mathbf{K}^T$  for all feature points in batch. Then, for each feature point  $i$ , we select its top- $k$  most similar neighbors (excluding itself) and compute the local density as:

$$\rho_i = \frac{1}{k} \sum_{j \in \mathcal{N}_k(i)} \mathbf{S}_{ij} \quad (4)$$

where  $\mathcal{N}_k(i)$  denotes the set of indices corresponding to the  $k$  most similar samples to the  $i$ -th sample (excluding  $i$  itself). The modulated  $\mathbf{W}$  still requires feature contrast enhancement, following the approach in TokenCut (Wang et al. 2022b). Specifically,  $\mathbf{W}_{ij}$  is set to 1 if  $\mathbf{W}_{ij} \geq \tau^{\text{ncut}}$ , and to  $1e^{-5}$  otherwise, where  $\tau^{\text{ncut}}$  is set to 0.15 by default.

Background regions typically exhibit sparse and relatively uniform features, allowing low-temperature areas to preserve the original similarity. In contrast, object interiors tend to have dense but uneven features, where high-temperature

areas suppress similarity more strongly, making intra-object similarities more consistent. Clearly, regions with uniform similarity are more likely to be grouped together, and our improvement leads to more accurate separation of foreground and background.

A similar idea is adopted by the clustering algorithm LDP-SC (Long et al. 2022), which combines local density peaks with NCut and demonstrates significant advantages when handling locally tree-structured data. This further validates the effectiveness and rationality of integrating density information into graph cut methods.

**Boundary Augmentation.** The attention map  $\mathbf{y}_1$  output by NCut tends to focus on a single object, which is the fundamental reason why MaskCut (Wang et al. 2023) applies the NCut algorithm multiple times to discover multiple objects. However, our goal is to obtain masks for multiple objects using NCut only once. This raises an important question: Are the less salient objects in the foreground being ignored by the SSM or the NCut algorithm? In fact, the potential objects are already represented, but it is difficult to assign those with relatively low attention to the foreground. From the first attention map (visualization of  $\mathbf{y}_1$ ) in 1, the following information can be easily extracted: 1) Regions with larger feature values are usually concentrated within parts of the objects. 2) In some object boundary areas, the feature values differ significantly from their surrounding regions.

To segment more objects, the salient regions within the foreground need to be expanded. Can boundary information be leveraged to achieve this? In practice, incorporating boundary information to refine original eigenvector  $\mathbf{y}_1$  has proven to be an effective approach. We propose a boundary-enhanced feature representation:

$$X_a = X - X_b \quad (5)$$

where  $X$  is the original eigenvector, and  $X_b$  is the boundary eigenvector obtained by calculating the difference between each point and its neighborhood:

$$X_b = \frac{1}{k} \sum_{n \in \mathcal{N}_k} |X - X_n|, \quad k \in \{4, 8\} \quad (6)$$

Here,  $\mathcal{N}_k$  denotes the  $k$ -neighborhood, which is set to 8 by default, and  $X_n$  represents the feature values within the neighborhood. To correctly compute boundary pixels, padding is applied to the four edges and four corners of the feature map. The padding regions should not introduce new groups, so the original boundary features are simply extended. Specifically, the feature values in the padding areas are set to those of the adjacent boundary pixels.

The third attention map in Figure 1 demonstrates the benefits of this improvement:

- The saliency of more objects is enhanced.
- The saliency of low-value small objects is suppressed.
- Closely located objects are less likely to be considered as a single entity.

First, we provide a theoretical analysis for the first two benefits.  $X_b$  focuses on regions with large feature differences, assigning higher attention to small areas around the

boundary between foreground and background, as well as to certain regions within the foreground. After optimizing the attention distribution using Equation 5, the attention  $X_a$  compared to  $X$  shows reduced focus within the foreground, making feature differences between regions inside the object smaller. This leads to an expansion of the salient foreground area. On the other hand, the regions on both sides of the boundary will “blend into” the background, and the boundary part of the foreground will turn into the background. This can be harmful for the segmentation of small objects. However, in most cases, it brings positive effects, as shown in the example from Figure 4. When an object has a very small area, this process causes such “noisy elements” to disappear. Next, we analyze the third benefit. For objects that are close to each other, there are usually small gaps between them. In these regions,  $X_b$  is relatively large while  $X_a$  is relatively small, making it easier for these areas to be treated as background.

Considering both comprehensive theoretical analysis and subsequent ablation study, boundary enhancement proves to be a strategy with more advantages than disadvantages. More visualizations of the computation process for this module are provided in the Appendix.

**Ranking-Based Instance Filter.** After extracting the foreground region from eigenvector using a segmentation threshold (as described in the *Preliminaries* section), the next step is to separate multiple objects from the foreground. To achieve this, we first apply 4-connectivity to perform connected component decomposition on the foreground region, treating each connected component as a candidate object. To select multiple salient objects from these candidates, we propose a feature rank-based connected component filtering strategy, which proceeds as follows:

1. Sort: Suppose there are  $N$  candidate object regions. Let  $s_i$  denote the feature sum of the  $i$ -th region. Sort all feature sums  $\{s_i\}_{i=1}^N$  in descending order to obtain the index sequence  $\{i_1, i_2, \dots, i_N\}$ .
2. Cumulative screening: Select the top-ranked objects one by one until the cumulative feature proportion reaches a predefined threshold:

$$\frac{\sum_{j=1}^k s_{i_j}}{\sum_{i=1}^N s_i} \geq \tau \quad (7)$$

where  $\tau \in (0, 1)$  is the feature preservation threshold.

3. Output: The masks corresponding to the top  $k$  selected objects.

Obviously, this strategy can extract the salient objects in the foreground in descending order of their feature significance. Unlike previous methods (Wang et al. 2023; Arica et al. 2024), our approach does not rely on CRF (Krähenbühl and Koltun 2011) in the object selection stage.

**Summary of New Modules.** The overall pipeline of CutOnce is illustrated in Figure 1. The first two improvements optimize the *input* and *output* of the NCut algorithm, respectively. Their underlying principle is consistent: enhancing the distinction between foreground and background to

Methods	CRF	ImageNet val					COCO val2017								
		#N	AP <sup>box</sup>	AP <sup>box</sup> <sub>50</sub>	AP <sup>box</sup> <sub>75</sub>	AR <sup>box</sup> <sub>100</sub>	#N	AP <sup>box</sup>	AP <sup>box</sup> <sub>50</sub>	AP <sup>box</sup> <sub>75</sub>	AR <sup>box</sup> <sub>100</sub>	AP <sup>mask</sup>	AP <sup>mask</sup> <sub>50</sub>	AP <sup>mask</sup> <sub>75</sub>	AR <sup>mask</sup> <sub>100</sub>
MaskCut	✓	1.9	10.6	20.3	10.0	27.7	1.9	3.9	7.9	3.3	7.7	3.1	6.8	2.5	6.5
VoteCut	✓	8.6	<b>20.9</b>	<b>36.2</b>	<b>20.0</b>	<b>45.0</b>	8.9	<b>5.5</b>	<b>10.7</b>	<b>4.9</b>	<b>12.2</b>	<b>4.5</b>	<b>9.3</b>	<b>3.9</b>	<b>10.3</b>
CutOnce(ours)	×	1.8	16.5	32.5	15.0	31.5	1.8	4.1	8.2	3.6	7.6	3.1	7.0	2.4	6.0
CutOnce*(ours)	✓	1.8	16.6	31.6	15.2	32.2	1.8	4.2	8.2	3.7	7.9	3.4	7.2	2.9	6.8

Table 2: **Evaluation of pseudo labels on ImageNet and COCO datasets.** #N denotes the average number of masks per image. The only difference between CutOnce and CutOnce\* lies in whether CRF is used for post-processing the masks.



Figure 2: **Qualitative comparison between our CutOnce and related methods on COCO val2017 dataset.** VoteCut only displays predicted masks with confidence scores no less than 0.5, while all masks are shown for other methods.

make the eigenvector distribution closer to the ideal, resembling the concept of contrastive learning. The third improvement targets the *graph partition* stage, effectively filtering out the most salient multiple objects. More importantly, it introduces only a single hyperparameter, making it significantly less reliant on engineering details compared to existing methods.

### Self-Training.

After training the detector with pseudo-labels generated by CutOnce, COLER further adopts a self-training strategy to improve model performance. This process is conducted solely within the ImageNet domain, consistent with the setup used in CutLER (Wang et al. 2023). In the  $t$ -th round of self-training ( $t \in 1, 2, \dots$ ), we first perform inference on the training data using the current model, retaining predicted masks with confidence scores higher than  $0.6 - 0.05t$  as high-quality pseudo-labels. To avoid label duplication and maintain diversity in the training data, we also select a subset of pseudo-labels from round  $(t-1)$  whose IoU with the current high-confidence predictions is less than 0.5. The final training labels for round  $t$  are obtained by merging these two sets.

## Experiments

This paper mainly uses AP<sub>50</sub> and AP as the evaluation metrics for presenting results. The Appendix reports all metrics across all datasets.

### Implementation Details

**Datasets.** In this paper, only the images from the validation set of ImageNet-1K (Deng et al. 2009) (50K images) are used for all training processes of the COLER model, with no manual annotations or any supervised pre-trained models employed in the training.

We evaluate on two subsets of the COCO (Lin et al. 2014) dataset, LVIS (Gupta, Dollár, and Girshick 2019), VOC (Everingham et al. 2010), KITTI (Geiger, Lenz, and Urtasun 2012), OpenImages (Kuznetsova et al. 2020) and Objects365 (Shao et al. 2019), resulting in a total of 7 benchmarks. COLER is a class-agnostic detector evaluated in a zero-shot manner across all datasets.

**CutOnce.** We resize images to  $480 \times 480$  pixels and use the ViT-B/8 [15] DINO [7] model by default to extract deep learning features. For the density-tune similarity module, the values of  $k$ ,  $T_0$ , and  $\alpha$  are set to 10, 1.0, and 0.5, respectively. The  $\tau$  for the filter is 0.95.

**Detector.** All training and inference are conducted on a single NVIDIA RTX 4090 GPU. All experiments are implemented on the detectron2 (Wu et al. 2019) platform using the widely adopted Cascade Mask R-CNN (Cai and Vasconcelos 2017) as detector. The detector is trained with masks and bounding boxes generated by CutOnce for 80K iterations with copy-paste augmentation (Ghiasi et al. 2021) and a batch size of 8. The learning rate is set to 0.01, weight decay to  $5 \times 10^{-5}$ , and momentum to 0.9.

**Self-Training.** We perform only one round of self-training. In this stage, the model is initialized with the weights from the previous phase and trained for 60K iterations. The learning rate is fixed at 0.005, and all other settings remain the same as in the previous stage.

**SOTA Comparison.** We compare our method with CutLER (Wang et al. 2023) and CuVLER (Arica et al. 2024), both of which satisfy the following criteria: 1) publicly available code with reproducible results; 2) support for object-level zero-shot instance segmentation.

### Pseudo Labels Evaluation

To evaluate the pseudo masks using the official COCO (Lin et al. 2014) evaluation tool, each annotation must be assigned a confidence score. The score has a significant impact on AP but does not affect AR. Since VoteCut (Arica et al. 2024) comes with its own scoring mechanism, we retain its original setting. To ensure a relatively fair comparison, we

Methods	Pretrain	Train #Rounds	COCO 20K				COCO val2017				LVIS			
			AP <sup>box</sup>	AP <sub>50</sub> <sup>box</sup>	AP <sup>mask</sup>	AP <sub>50</sub> <sup>mask</sup>	AP <sup>box</sup>	AP <sub>50</sub> <sup>box</sup>	AP <sup>mask</sup>	AP <sub>50</sub> <sup>mask</sup>	AP <sup>box</sup>	AP <sub>50</sub> <sup>box</sup>	AP <sup>mask</sup>	AP <sub>50</sub> <sup>mask</sup>
CutLER	IN train	1 + 3	12.5	22.4	<b>10.0</b>	19.6	12.3	21.9	9.7	18.9	4.5	8.4	3.5	6.7
CuVLER	IN val	1	<b>12.7</b>	23.5	<b>10.0</b>	20.1	<b>12.6</b>	23.0	<b>9.8</b>	19.3	4.5	8.6	3.6	6.9
COLER(ours)	IN val	1 + 1	12.6	<b>24.1</b>	9.8	<b>20.5</b>	12.5	<b>23.8</b>	9.6	<b>20.1</b>	<b>4.6</b>	<b>9.2</b>	<b>3.7</b>	<b>7.3</b>
vs. <i>SOTA</i>			-0.1	+0.6	-0.2	+0.4	-0.1	+0.8	-0.2	+0.8	+0.1	+0.6	+0.1	+0.4

Table 3: **Zero-shot evaluation of details across three COCO-based datasets.** Pretrain, IN and 1 + 3 denote training dataset, ImageNet-1K and one training plus three rounds of in-domain self-training, respectively.

Datasets Metrics	Avg.		COCO		COCO20K		LVIS		VOC		KITTI		OpenImages		Objects365	
	AP <sub>50</sub>	AP	AP <sub>50</sub>	AP	AP <sub>50</sub>	AP	AP <sub>50</sub>	AP	AP <sub>50</sub>	AP	AP <sub>50</sub>	AP	AP <sub>50</sub>	AP	AP <sub>50</sub>	AP
CutLER	21.0	11.3	21.9	12.3	22.4	12.5	8.4	4.5	36.9	20.2	18.4	8.5	17.3	9.7	21.6	<b>11.4</b>
CuVLER	21.2	<b>11.4</b>	23.0	<b>12.6</b>	23.5	<b>12.7</b>	8.6	4.5	<b>39.4</b>	<b>22.3</b>	13.0	5.1	<b>19.6</b>	<b>11.6</b>	21.6	10.9
COLER(ours)	<b>22.3</b>	<b>11.4</b>	<b>23.8</b>	12.5	<b>24.1</b>	12.6	<b>9.2</b>	<b>4.6</b>	39.1	20.5	<b>20.8</b>	<b>8.8</b>	16.7	9.3	<b>22.3</b>	11.2
vs. <i>SOTA</i>	+1.0	0.0	+0.8	-0.1	+0.6	-0.1	+0.6	+0.1	-0.3	-1.8	+2.4	+0.3	-2.9	-2.3	+0.7	-0.2

Table 4: **Zero-shot unsupervised object detection evaluation on all datasets.** ‘‘Avg.’’ denotes the average value.

apply the same scoring scheme to both MaskCut (Wang et al. 2023) and CutOnce. The reason is that both methods output masks in descending order of object saliency and treat all outputs as ‘‘ground truth’’. For multiple masks associated with the same image, we adopt a linearly decreasing score assignment scheme. The confidence score for each mask is calculated as follows:

$$\text{score} = \begin{cases} 1.0 & \text{if } N = 1 \\ 1.0 - \frac{k}{2N - 2} & \text{if } N > 1 \end{cases} \quad (8)$$

where  $N$  denotes the total number of masks for a given image, and  $k$  represents the index of the current mask ( $k = 0, 1, \dots, N - 1$ ). This ensures that the first mask always receives the highest confidence score of 1.0, while the last mask is assigned a score of 0.5.

Table 2 presents the quantitative comparisons of different methods, and Figure 2 shows the corresponding qualitative results. On ImageNet val, all metrics of CutOnce lie between those of MaskCut and VoteCut. On COCO val2017, CutOnce shows poor performance in  $\text{AR}_{100}^{\text{mask}}$ . When CutOnce applies CRF (Krähenbühl and Koltun 2011) to refine the masks, the improvement on COCO is noticeable, with all metrics surpassing those of MaskCut.

It can be seen from Figure 2 that CutOnce always exhibits more robust performance. Judging from the box boundaries, CutOnce demonstrates good localization ability, detecting the fewest objects but also making fewer false predictions. Since CutOnce does not use CRF for post-processing, its boundaries are slightly coarse.

### Unsupervised Zero-shot Evaluations

We evaluate COLER on 7 different benchmarks, containing a variety of object categories and image styles, to validate its effectiveness as a general unsupervised method. More detailed results are provided in the Appendix.



Figure 3: **Qualitative comparison between our COLER and related methods on COCO val2017 dataset.** Only predicted results with a confidence score of no less than 0.5 are shown (excluding ground truth).

**Detailed in COCO Datasets.** Since only COCO 20K, COCO val2017, and LVIS provide segmentation annotations and all three are derived from the COCO dataset, we first conduct a comprehensive evaluation on these datasets. The results are reported in Table 3. Compared to other methods (Wang et al. 2023; Arica et al. 2024), COLER achieves comparable results on COCO and COCO 20K, with consistently higher  $\text{AP}_{50}$  than previous approaches, though its overall AP is lower than prior SOTA methods. Surprisingly, on the densely annotated LVIS dataset, COLER outperforms all previous methods across all metrics.

Figure 3 shows the qualitative results of COLER compared with related methods. Obviously, COLER often de-

$\tau$	0.8	0.9	<b>0.95</b>	0.99	$k$	3	5	<b>10</b>	20	$T_0$	0.8	<b>1.0</b>	1.2	$\alpha$	0.3	<b>0.5</b>	0.7
$AP_{50}^{\text{mask}}$	17.3	18.5	<b>19.2</b>	17.1	$AP_{50}^{\text{mask}}$	18.5	18.9	<b>19.2</b>	18.3	$AP_{50}^{\text{mask}}$	18.1	<b>19.2</b>	18.5	$AP_{50}^{\text{mask}}$	18.3	<b>19.2</b>	18.6

Table 5: **Ablation study of CutOnce hyperparameters on COCO val2017 dataset.**  $\tau$  denotes the feature preservation ratio in the filter, while  $k$ ,  $T_0$ , and  $\alpha$  are parameters related to the adaptive edge weight matrix.

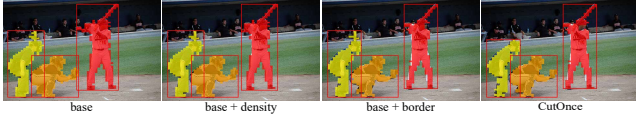


Figure 4: **Ablation study on the components of CutOnce.** *Base* denotes the baseline version without any enhancements to the NCut algorithm.

tests more useful instances, including some that are not annotated in the ground truth. In certain cases, closely located objects are not grouped as a single entity, which reflects the desirable property inherited from CutOnce.

**Object Detection.** In Table 4, we report COLER’s object detection performance across all datasets. On average, COLER achieves a significant improvement in  $AP_{50}$ , while its AP remains nearly the same as previous methods. This suggests that COLER performs well in coarse object localization but is less effective in precise localization. On most datasets, its performance is comparable to that of prior state-of-the-art methods. However, on the more challenging datasets such as LVIS and KITTI, COLER delivers notably strong results. In general, our method shows consistent performance across all datasets.

## Ablation Study

Table 5 reports the ablation study of the hyperparameters introduced by CutOnce, where the detector is trained only once. Figure 4 visualizes the ablation study of the two modules introduced in CutOnce for enhanced object discovery. It is evident that when both optimization modules for NCut are combined, the top three salient objects are well preserved, with accurate localization and segmentation. In contrast, removing either module often leads to poor mask boundaries for certain objects.

Table 6 reports the impact of each component in COLER on the final results across two datasets. Each component contributes to performance improvements to varying degrees, but the boundary enhancement module proves to be the most critical for boosting overall performance. Additionally, copy-paste augmentation (Ghiasi et al. 2021) and self-training during the training process also contribute significantly to the overall improvement of COLER.

Table 7 reports the impact of the number of self-training rounds on the final performance of COLER. The first round of self-training improves all metrics, while the second round causes some of them to drop.

Methods	COCO		KITTI	
	$AP_{50}^{\text{mask}}$	$AP_{50}^{\text{mask}}$	$AP_{50}^{\text{box}}$	$AP_{50}^{\text{box}}$
CutOnce (base) + Det.	7.5	15.7	6.3	15.2
+ similarity tune	7.7	16.1	6.6	15.8
+ boundary augment	8.6	18.0	7.5	18.6
+ copy-paste	9.2	19.2	7.6	18.8
+ self-training (COLER)	<b>9.6</b>	<b>20.1</b>	<b>8.8</b>	<b>20.8</b>

Table 6: **Ablation analysis of COLER components on COCO val2017 and KITTI datasets.** *CutOnce (base)* denotes the version without NCut algorithm enhancements, and “Det.” refers to the Cascade Mask R-CNN detector.

Round	COCO				KITTI	
	$AP_{50}^{\text{box}}$	$AP_{50}^{\text{box}}$	$AP_{50}^{\text{mask}}$	$AP_{50}^{\text{mask}}$	$AP_{50}^{\text{box}}$	$AP_{50}^{\text{box}}$
0	12.2	23.2	9.2	19.6	7.6	18.8
<b>1</b>	<b>12.5</b>	<b>23.8</b>	9.6	<b>20.1</b>	8.8	<b>20.8</b>
2	12.2	23.4	<b>9.8</b>	19.9	<b>8.9</b>	20.7

Table 7: **Number of self-training rounds used by COLER on COCO val2017 and KITTI datasets.**

## Discussion

CutOnce does not show an advantage over existing state-of-the-art methods. However, after using the pseudo masks for training, our method demonstrates a certain advantage. As shown in Table 2, CutOnce produces the fewest masks but achieves a relatively high AP. Although VoteCut (Arica et al. 2024) leads across all metrics, its predictions contain a large number of inaccurate annotations, which can negatively impact model training.

Despite the strong performance of COLER, it also has several limitations: 1) When multiple objects in an image are highly overlapping, COLER still struggles to separate them effectively. It also fails to handle occluded objects. 2) In some cases, CutOnce can distinguish spatially adjacent objects, whereas COLER fails to do so. To address these limitations, we plan to explore end-to-end unsupervised object discovery in future work.

## Conclusion

We propose CutOnce, a novel training-free method for unsupervised object discovery that efficiently and accurately partitions multiple instances within a single image. In particular, the boundary enhancement strategy stands out as the simplest yet most effective improvement in this work, and we believe it holds great potential for broader applica-

tions in the future. We also introduce COLER, a zero-shot model trained using masks generated by CutOnce. With only ImageNet-1K as the source domain and relatively low cost, COLER surpasses previous state-of-the-art models on multiple benchmarks.

## References

- Arice, S.; Rubin, O.; Gershov, S.; and Laufer, S. 2024. CuVLER: Enhanced Unsupervised Object Discoveries through Exhaustive Self-Supervised Transformers. In *CVPR*, 23105–23114.
- Cai, Z.; and Vasconcelos, N. 2017. Cascade R-CNN: Delving Into High Quality Object Detection. In *ICCV*, 6154–6162.
- Caron, M.; Touvron, H.; Misra, I.; Jégou, H.; Mairal, J.; Bojanowski, P.; and Joulin, A. 2021. Emerging Properties in Self-Supervised Vision Transformers. *ICCV*, 9630–9640.
- Couairon, P.; Shukor, M.; HAUGEARD, J.-E.; Cord, M.; and THOME, N. 2024. DiffCut: Catalyzing Zero-Shot Semantic Segmentation with Diffusion Features and Recursive Normalized Cut. In *NeurIPS*.
- Deng, J.; Dong, W.; Socher, R.; Li, L.-J.; Li, K.; and Fei-Fei, L. 2009. ImageNet: A large-scale hierarchical image database. In *CVPR*, 248–255.
- Dosovitskiy, A.; Beyer, L.; Kolesnikov, A.; Weissenborn, D.; Zhai, X.; Unterthiner, T.; Dehghani, M.; Minderer, M.; Heigold, G.; Gelly, S.; Uszkoreit, J.; and Houlsby, N. 2020. An Image is Worth 16x16 Words: Transformers for Image Recognition at Scale. In *ICLR*.
- Everingham, M.; Van Gool, L.; Williams, C. K.; Winn, J.; and Zisserman, A. 2010. The pascal visual object classes (voc) challenge. *IJCV*, 303–338.
- Geiger, A.; Lenz, P.; and Urtasun, R. 2012. Are we ready for autonomous driving? The KITTI vision benchmark suite. In *CVPR*, 3354–3361.
- Ghiasi, G.; Cui, Y.; Srinivas, A.; Qian, R.; Lin, T.-Y.; Cubuk, E. D.; Le, Q. V.; and Zoph, B. 2021. Simple copy-paste is a strong data augmentation method for instance segmentation. In *Proceedings of the IEEE/CVF conference on computer vision and pattern recognition*, 2918–2928.
- Gupta, A.; Dollár, P.; and Girshick, R. B. 2019. LVIS: A Dataset for Large Vocabulary Instance Segmentation. In *CVPR*, 5351–5359.
- Krähenbühl, P.; and Koltun, V. 2011. Efficient Inference in Fully Connected CRFs with Gaussian Edge Potentials. In *NeurIPS*.
- Kuznetsova, A.; Rom, H.; Alldrin, N.; Uijlings, J.; Krasin, I.; Pont-Tuset, J.; Kamali, S.; Popov, S.; Mallocci, M.; Kolesnikov, A.; et al. 2020. The open images dataset v4: Unified image classification, object detection, and visual relationship detection at scale. *IJCV*, 1956–1981.
- Lin, T.-Y.; Maire, M.; Belongie, S. J.; Hays, J.; Perona, P.; Ramanan, D.; Dollár, P.; and Zitnick, C. L. 2014. Microsoft COCO: Common Objects in Context. In *ECCV*.
- Liu, Y.; and Gould, S. 2024. Unsupervised Dense Prediction Using Differentiable Normalized Cuts. In *ECCV*, 287–304.
- Long, Z.; Gao, Y.; Meng, H.; Yao, Y.; and Li, T. 2022. Clustering based on local density peaks and graph cut. *Information Sciences*, 600: 263–286.
- Maji, S.; Vishnoi, N. K.; and Malik, J. 2011. Biased normalized cuts. In *CVPR*, 2057–2064. IEEE.
- Rambhatla, S. S.; Misra, I.; Chellappa, R.; and Shrivastava, A. 2023. MOST: Multiple Object Localization with Self-supervised Transformers for Object Discovery. In *ICCV*, 15777–15788.
- Ronneberger, O.; Fischer, P.; and Brox, T. 2015. U-net: Convolutional networks for biomedical image segmentation. In *International Conference on Medical image computing and computer-assisted intervention*, 234–241. Springer.
- Shao, S.; Li, Z.; Zhang, T.; Peng, C.; Yu, G.; Zhang, X.; Li, J.; and Sun, J. 2019. Objects365: A large-scale, high-quality dataset for object detection. In *ICCV*, 8430–8439.
- Shi, J.; and Malik, J. 2000. Normalized Cuts and Image Segmentation. *IEEE Transactions on Pattern Analysis and Machine Intelligence*, 888–905.
- Sick, L.; Engel, D.; Hartwig, S.; Hermosilla, P.; and Ropinski, T. 2024. CutS3D: Cutting Semantics in 3D for 2D Unsupervised Instance Segmentation. arXiv:2411.16319.
- Siméoni, O.; Puy, G.; Vo, H. V.; Roburin, S.; Gidaris, S.; Bursuc, A.; Pérez, P.; Marlet, R.; and Ponce, J. 2021. Localizing Objects with Self-Supervised Transformers and no Labels. In *BMVC*.
- Siméoni, O.; Sekkat, C.; Puy, G.; Vobecký, A.; Zablocki, É.; and Pérez, P. 2022. Unsupervised Object Localization: Observing the Background to Discover Objects. In *CVPR*, 3176–3186.
- Simeoni, O.; Zablocki, E.; Gidaris, S.; Puy, G.; and Perez, P. 2025. Unsupervised object localization in the era of self-supervised vits: A survey. *International Journal of Computer Vision*, 133(2): 781–808.
- Wang, X.; Girdhar, R.; Yu, S. X.; and Misra, I. 2023. Cut and Learn for Unsupervised Object Detection and Instance Segmentation. In *CVPR*, 3124–3134.
- Wang, X.; Yu, Z.; Mello, S. D.; Kautz, J.; Anandkumar, A.; Shen, C.; and Álvarez, J. M. 2022a. FreeSOLO: Learning to Segment Objects without Annotations. In *CVPR*, 14156–14166.
- Wang, X.; Zhang, R.; Shen, C.; Kong, T.; and Li, L. 2020. Dense Contrastive Learning for Self-Supervised Visual Pre-Training. *CVPR*, 3023–3032.
- Wang, Y.; Shen, X.; Hu, S. X.; Yuan, Y.; Crowley, J. L.; and Vafreydaz, D. 2022b. Self-Supervised Transformers for Unsupervised Object Discovery using Normalized Cut. In *CVPR*, 14543–14553.
- Wu, Y.; Kirillov, A.; Massa, F.; Lo, W.-Y.; and Girshick, R. 2019. Detectron2. <https://github.com/facebookresearch/detectron2>.

## Appendix

### Advancing COLER

COLER can achieve good performance without relying on CRF (Krähenbühl and Koltun 2011), but applying CRF can further improve the results. *Since extensive ablation studies are required in the main text and considering the time constraints for experiments, CRF post-processing is not adopted by default.* The related results are reported in Table 8. While CRF does not improve  $AP_{50}$ , it enhances the overall AP, indicating its positive effect on high-precision localization.

CRF	Avg. OD		Avg. IS	
	$AP_{50}^{\text{box}}$	$AP^{\text{box}}$	$AP_{50}^{\text{mask}}$	$AP^{\text{mask}}$
×	21.8	11.1	15.6	7.4
✓	21.8	<b>11.3</b>	15.6	<b>7.5</b>

Table 8: **Effect of CRF post-processing on COLER performance.** "Avg.", OD, and IS denote the average, object detection, and instance segmentation, respectively. The results are based on a single training run of COLER.



Figure 5: **Visualization of the computation process of CutOnce.** The first column (top to bottom) shows the original image, CutOnce prediction, and CutOnce with post-processing. The second to fourth columns show the raw eigenvector, boundary eigenvector, the difference between the two, and the corresponding foreground-background binary maps and connected component maps.

### Datasets used for evaluation

**COCO** (Lin et al. 2014) (Microsoft Common Objects in Context) is a large-scale dataset for object detection and segmentation. In this paper, COCO refers to the 5k images from the 2017 validation set.

**COCO 20K** (Lin et al. 2014) contains 19,817 images, a subset of COCO train2014. Many previous unsupervised methods (Wang et al. 2022b, 2023; Arica et al. 2024) have used this dataset to evaluate model performance.

datasets	testing data	seg label	#images	avg. # obj.
COCO	val2017	✓	5,000	7.4
COCO20K	train2014	✓	20,000	7.3
LVIS	val	✓	19,809	12.4
Pascal VOC	trainval07	×	9,963	3.1
KITTI	trainval	×	7,521	4.7
OpenImages V7	val	×	41,620	7.3
Object365 V2	val	×	80,000	15.5
ImageNet	val	×	50,000	1.6

Table 9: **Summary of datasets used for zero-shot evaluation (except ImageNet).** "avg. # obj." denotes the average number of annotations per image.

**LVIS** (Gupta, Dollár, and Girshick 2019): (Large Vocabulary Instance Segmentation) is a dataset for long-tail instance segmentation. It contains 2.2 million high-quality instance masks of over 1,000 entry-level object categories, collected based on the COCO dataset. In this paper, LVIS refers to the 19,809 images in the validation set.

**VOC** (Everingham et al. 2010) (PASCAL Visual Object Classes) is a widely used benchmark for object detection. We evaluate on its `trainval07` split.

**KITTI** (Geiger, Lenz, and Urtasun 2012) (Karlsruhe Institute of Technology and Toyota Technological Institute) is one of the most popular datasets for mobile robotics and autonomous driving. We evaluate on its `trainval` split.

**OpenImages V7** (Kuznetsova et al. 2020) contains multiple tasks, including image classification, object detection, instance segmentation, and visual relationship detection. We evaluate on over 40K images from the `val` split.

**Object365 V2** (Shao et al. 2019) provides a supervised object detection benchmark with a focus on diverse objects in the natural world. We evaluate on 80K images from the `val` split.

The summary of these datasets used for zero-shot evaluation is provided in Table 9.

### Other Visualizations

Figure 5 shows a visualization of the intermediate computation process of CutOnce’s boundary enhancement module. Obviously, the mechanism of this module is easy to understand and delivers immediate results.

Figure 6 demonstrates the strong capability of CutOnce in segmenting multiple objects, which previous methods were unable to detect in such quantity.

Table 10 and Table 11 present the zero-shot evaluation results on unsupervised instance segmentation and object detection tasks across various datasets, respectively.

Datasets	$AP^{\text{mask}}$	$AP_{50}^{\text{mask}}$	$AP_{75}^{\text{mask}}$	$AP_S^{\text{mask}}$	$AP_M^{\text{mask}}$	$AP_L^{\text{mask}}$	$AR_1^{\text{mask}}$	$AR_{10}^{\text{mask}}$	$AR_{100}^{\text{mask}}$	$AR_S^{\text{mask}}$	$AR_M^{\text{mask}}$	$AR_L^{\text{mask}}$
COCO	9.6	20.1	8.5	2.3	10.5	21.5	5.6	16.3	25.4	9.5	31.2	44.9
COCO20K	9.8	20.5	8.4	2.6	10.5	21.6	5.6	16.5	25.6	9.7	31.6	44.7
LVIS	3.7	7.3	3.2	1.5	6.9	12.0	2.1	7.9	16.1	6.3	29.2	41.8

Table 10: **Unsupervised instance segmentation results on all benchmarks in this work.**

Datasets	$AP^{\text{box}}$	$AP_{50}^{\text{box}}$	$AP_{75}^{\text{box}}$	$AP_S^{\text{box}}$	$AP_M^{\text{box}}$	$AP_L^{\text{box}}$	$AR_1^{\text{box}}$	$AR_{10}^{\text{box}}$	$AR_{100}^{\text{box}}$	$AR_S^{\text{box}}$	$AR_M^{\text{box}}$	$AR_L^{\text{box}}$
COCO	12.5	23.8	11.9	4.0	13.5	27.7	6.6	19.8	32.0	13.2	38.7	55.8
COCO20K	12.6	24.1	11.8	4.3	13.3	27.6	6.6	20.0	32.2	13.5	38.9	55.8
LVIS	4.6	9.2	4.1	2.4	8.6	15.5	2.4	9.5	20.0	8.7	34.9	51.6
VOC	20.5	39.1	19.6	2.7	8.2	31.5	15.9	33.2	44.6	19.3	36.5	54.5
KITTI	8.8	20.8	6.2	1.2	6.2	17.4	6.3	19.7	29.7	17.4	26.8	42.1
OpenImages	9.3	16.7	9.2	0.2	1.9	14.6	6.6	16.5	27.1	4.1	19.6	34.6
Objects365	11.2	22.6	9.8	2.6	10.5	19.1	2.8	15.0	32.0	11.7	34.6	45.9

Table 11: **Unsupervised object detection results on all benchmarks in this work.**

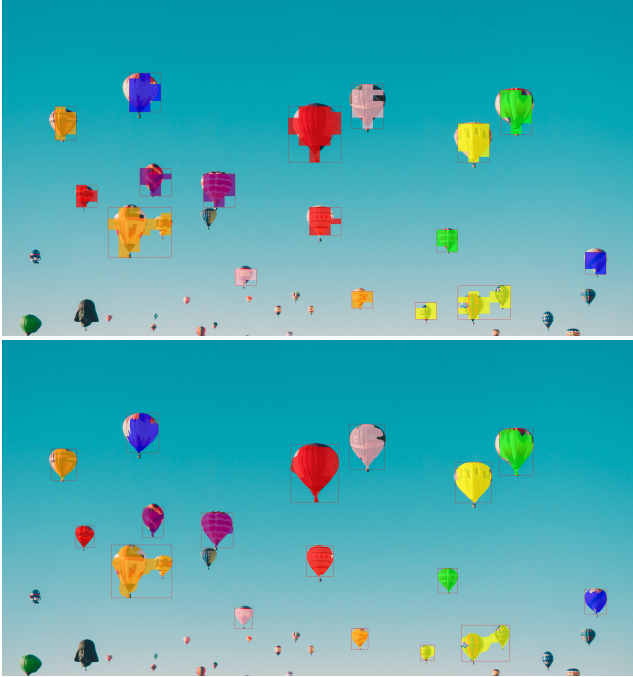


Figure 6: The first row shows the results of CutOnce, and the second row presents the results of CutOnce with post-processing, with each identifying 17 objects.